Polymer Chemistry

PAPER

View Article Online
View Journal | View Issue

Cite this: *Polym. Chem.*, 2025, **16**, 4731

Ethylene and alkyl acrylate copolymers made-to-order using dynamic cation switching polymerization and evidence for improved polymer degradability with low polar group density

Tuhin Ganguly, Lorenzo C. Ruiz De Castilla, Rumela Adhikary and Loi H. Do *

The industrial synthesis of functional polyolefins relies on free radical polymerization, which requires high temperature and pressure and offers poor microstructure control. Herein, we report a cation-switching strategy to access ethylene and alkyl acrylate copolymers with made-to-order molecular weight, molecular weight distribution, and polar monomer density, tunable within a catalyst-dependent range. This precision was achieved by exploiting the cation exchange dynamics between M^+ and M'^+ (where M^+, M'^+ = Li^+, Na^+, K^+, or Cs^+, and $M \neq M'$) with our nickel phenoxyphosphine-polyethylene glycol catalyst. Under non-switching conditions, copolymerization of ethylene and methyl acrylate (MA) using our nickel catalyst in the presence of M^+ and M'^+ salts afforded ethylene-MA copolymers (EMA) with adjustable molecular weight distributions based on the ratio of $M^+ : M'^+$ employed. Under dynamic cation switching conditions, this catalyst system yielded monomodal EMA with molecular weight and MA incorporation that can be varied independently. Studies of the EMA revealed that while they retain the thermal and mechanical properties of polyethylene having the same molecular weight, increasing the MA per chain by as few as 1–3 units leads to measurable increase in their wettability and susceptibility toward oxidative cleavage. This work adds to a growing body of evidence suggesting that ethylene-based materials can be designed for improved degradability without compromising their performance.

Received 17th August 2025,
Accepted 1st October 2025

DOI: 10.1039/d5py00819k

rsc.li/polymers

Introduction

Research in polyolefin synthesis continues to thrive due to the high demand for durable, inexpensive, and high-performing plastic across many industrial sectors.[1–3] Interest in functional polyolefins stems from their enhanced properties (*e.g.*, increased flexibility, blending compatibility, adhesiveness, *etc.*) relative to that of polyethylene (PE).[4–6] A variety of ethylene-alkyl acrylate copolymers (EAA) have been used in applications such as food packaging, films, sporting goods, personal care products, and others (Chart 1A). Some examples of commercial EAA include ELVALOY AC from the Dow Chemical Company,[7] Ebantix from Repsol,[8] and Optema from ExxonMobil Chemical.[9] These copolymers are synthesized using free radical polymerization (Chart 1B, option I), which must be performed at high pressure (~150–350 MPa) and temperature (>160 °C).[10]

Another approach to prepare EAA is through the coordination–insertion copolymerization of ethylene and alkyl acrylate using transition metal catalysts (Chart 1B, option II).[11–17] This method can provide EAA with narrow dispersity ($Đ$ < 2), variable polar monomer content, and even ultra-high molecular weight (M_n > 10^3 kg mol^{-1}).[18] However, obtaining EAA with user-defined specifications remains a significant challenge. For example, increasing the alkyl acrylate concentration in the copolymerization reaction can enhance the polar content in the resulting polymer but the molecular weight typically decreases and *vice versa*.[19–22] Thus, independently varying a single parameter in copolymerization, such as MW, MW distribution (MWD), or polar group incorporation, without impacting another is difficult to achieve.

To overcome the limitations of a one catalyst-one polymer paradigm,[23] our group has focused on the development of cation-tunable polymerization catalysts.[24–26] Unlike other strategies that rely on light,[27] redox agents,[28–31] or boranes,[32,33] the use of secondary metal cations with polymerization catalysts offers the potential to access more than two reactivity states.[34] For example, metal cations can differ in charge, Lewis acidity, and size, which can modulate a catalyst's steric and electronic properties to different extent. A variety of Ni/Pd catalyst plat-

Department of Chemistry, University of Houston, 4800 Calhoun Road, Houston, TX 77004, USA. E-mail: loido@uh.edu

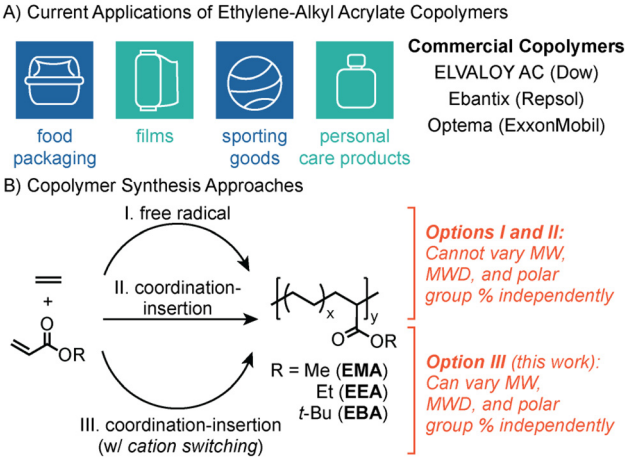

Chart 1 Current applications of ethylene-alkyl acrylate copolymers (A) and various options available to synthesize them (B). Our approach using dynamic cation switching polymerization enables the preparation of EAA with precisely controlled MW, MWD, and alkyl acrylate incorporation.

forms have been demonstrated to be cation-tunable, including those based on *P,O*-,[25,26,35–37] *N,O*-,[24,38] and *C,O*-donors.[39] Our recent discovery that cation exchange equilibria could be manipulated to influence the coordination–insertion of non-living polymerization catalysts affords another level of control.[40] Under non-switching conditions, the polymerization of ethylene using our nickel phenoxyphosphine polyethylene glycol (PEG) catalysts with M^+ and M'^+ (where M^+, M'^+ = Li^+, Na^+, K^+, or Cs^+; and $M^+ \neq M'^+$) yielded bimodal PE with adjustable MWD depending on the $M^+ : M'^+$ ratio employed. In contrast, under dynamic cation switching conditions, the same catalyst system generated monomodal PE with tunable MW as a function of the $M^+ : M'^+$ ratio. However, these studies were performed in the presence of only ethylene so it was unclear whether polar monomers would be compatible with this polymerization strategy.

In this work, we successfully expanded the application of dynamic cation switching to ethylene and alkyl acrylate copolymerization, enabling for the production of functional polyolefins with high precision (Chart 1B, option III). We demonstrate that ethylene-methyl acrylate copolymers (EMA) can be made-to-order with specific MW, MWD, and polar group incorporation, tunable within a catalyst-dependent range. Having access to a series of systematically varied EMA allowed us to interrogate their structure–function relationships, offering new insights into the properties of this important class of polymers.

Results and discussion

Catalyst selection and metal cation binding

Previously, we demonstrated that nickel phenoxyphosphine-PEG complexes readily formed adducts with alkali ions to generate highly active heterobimetallic species capable of polymerizing ethylene.[26,40,41] The catalyst activity and polymer MW and branching were dependent on the identity of M^+. The first-generation catalyst **Ni1** contained bis(2-methoxyphenyl)-phosphine moieties (Fig. 1A)[26,41] whereas the second-generation catalyst **Ni2** contained bis(2,6-dimethoxyphenyl)-phosphine moieties (Scheme S1).[40] Although **Ni2** provided polymers with higher MW than **Ni1**, we chose the latter for this proof-of-concept study because it is less air-sensitive and can be obtained in greater yield. Complex **Ni1** was prepared as described in our earlier work[26] but with modifications to a few steps to improve the synthetic efficiency (see SI for details).

Although we have shown that the cation exchange rates between our Ni complexes and M^+ can be controlled by solvent polarity (*i.e.*, polar mixtures facilitate fast exchange whereas non-polar mixtures facilitate slow exchange),[40] we were unsure whether polar monomers would affect these rates. To interrogate this possibility, we conducted a series of cation binding studies. In these experiments, **Ni1** was dissolved in toluene-d_8/Et_2O (48 : 2) and then various amounts of $NaBAr^F{}_4$ were added.

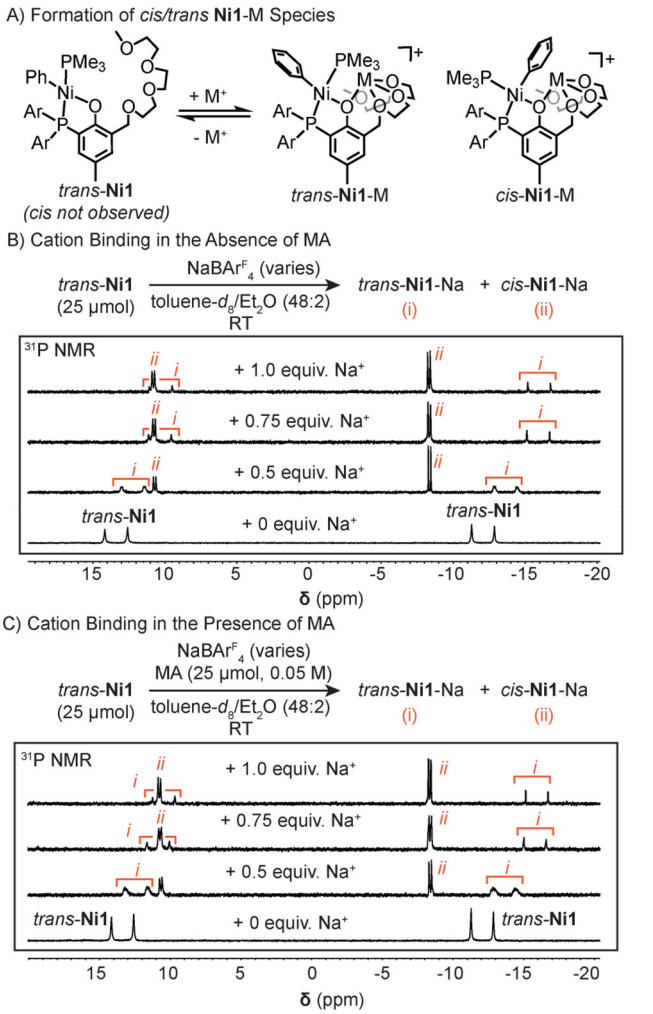

Fig. 1 Addition of M^+ to **Ni1** leads to the formation of *cis* and *trans* **Ni1**–M species in solution (A). ^{31}P NMR spectra (202 MHz) of **Ni1** after the addition of up to 1.0 equiv. of $NaBAr^F{}_4$ in the absence (B) and presence (C) of MA. Ar = 2-methoxyphenyl.

The mixtures were stirred for 10 min and then analyzed by ^{31}P NMR spectroscopy. The starting **Ni1** complex showed two doublets centered at −12.1 and 13.4 ppm (J = 319 Hz), consistent with having a *trans* arrangement of the two phosphine donors around the nickel square plane (Fig. 1A, *trans*-**Ni1**).[41,42] The *cis*-**Ni1** isomer, in which the phosphine ligands are adjacent to each other in the nickel center, was not observed. In the absence of methyl acrylate (MA), the addition of up to 1.0 equiv. of Na^+ resulted in the appearance of two sets of signals (Fig. 1B). The first set of peaks shifted upfield as increasing quantities of Na^+ were added, ultimately centering at −15.9 and 10.3 ppm (J = 319 Hz). We propose that these peaks arise from signaling average of *trans*-**Ni1** and *trans*-**Ni1**–Na species interconverting on the NMR timescale, suggesting that cation exchange occurs readily in this solvent mixture. The second set of signals at −8.4 and 10.8 ppm grew in intensity but did not shift when greater amounts of Na^+ were introduced. These resonances were assigned to the two phosphines in *cis*-**Ni1**–Na based on their J coupling constant of 34 Hz.[42] Because the starting nickel species does not exist in the *cis* form, there is no possibility of *cis*-**Ni1** and *cis*-**Ni1**–Na equilibration.

Next, the binding of Na^+ to **Ni1** was evaluated in the presence of 0.05 M methyl acrylate in toluene-d_8/Et_2O (48 : 2) (Fig. 1C). We observed that the ^{31}P NMR spectra of the **Ni1** and Na^+ samples with and without MA additives were nearly identical, indicating that the presence of polar monomers at the concentration tested had minimal effects on the cation binding dynamics. Additional experiments conducted using **Ni1** and $CsBAr^F{}_4$ in toluene-d_8/Et_2O (48 : 2) showed similar behavior (Fig. S3). Specifically, the treatment of **Ni1** with Cs^+ led to the formation of heterobimetallic *trans*-**Ni1**–Cs and *cis*-**Ni1**–Cs species. Once again, signal averaging between the *trans*-**Ni1** and *trans*-**Ni1**–Cs peaks suggests that cation exchange is fast in this solvent mixture. However, under catalytic conditions, the MA : catalyst stoichiometry is typically 1250 : 1 rather than 1 : 1 so we expect that MA will have a more significant impact on the cation binding behavior in polymerization (*vide infra*). Although it might be possible to use other polar co-solvents such as tetrahydrofuran or dioxane, we prefer diethyl ether because it is less coordinating, minimizing possible catalyst inhibition effects.

Ethylene and alkyl acrylate copolymerization

The nickel phenoxyphosphine complexes are among the highest performing catalysts for ethylene and polar vinyl monomer copolymerization reported to date.[18,43–46] Encouraged by these reports, we proceeded to evaluate the reactivity of **Ni1**–M (where M^+ = Li^+, Na^+, K^+, or Cs^+) toward ethylene and alkyl acrylates. In our initial studies, we combined **Ni1** (2 μmol), $NaBAr^F{}_4$ (4 μmol), $Ni(COD)_2$ (8 μmol), and MA (2.5 mmol, 0.05 M) in toluene/Et_2O (48 : 2) under ethylene at 30 °C (Fig. 2; Table S1, entry 3). After 0.5 h, the reaction was quenched with acid and the resulting white solid was characterized by ^{1}H NMR spectroscopy. The broad peaks at ∼2.5 and 3.7 ppm were assigned to in-chain methyl ester groups,[17,45,47] confirming that the desired EMA was obtained (Fig. S39).

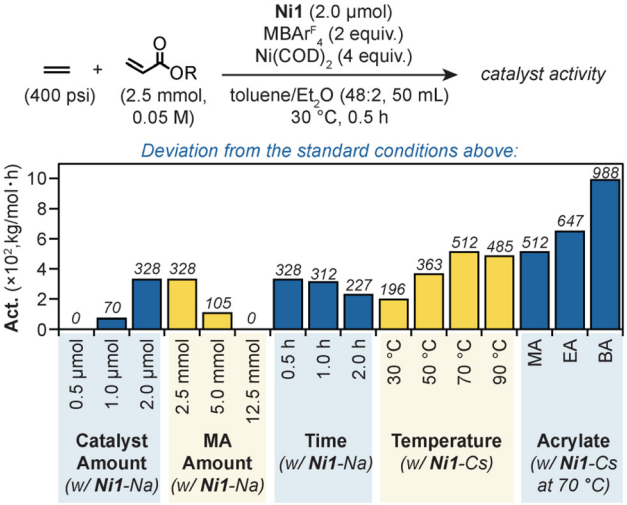

Fig. 2 Determining the optimal reaction conditions for ethylene and alkyl acrylate copolymerization using the **Ni1**–M catalysts. These values are obtained from the average of at least duplicate experiments. R = Me, Et, or *t*-Bu.

Further characterization of the copolymer showed that it has an average molar mass (M_n) of 2.2 kg mol^{-1} with 1.08 mol% incorporation of MA and dispersity ($Đ$) of 1.1. We found that decreasing the **Ni1** catalyst loading to 0.5 μmol (Table S1) or increasing the MA concentration to 0.25 M (12.5 mmol, Table S2) resulted in no product. Because MA can inhibit the nickel catalyst *via* coordination by its oxygen donor rather than C=C bond, increasing the MA : catalyst ratio often leads to lower catalyst activity.[19,21,48] Finally, extending the polymerization time from 0.5 to 2.0 h led to a reduction in catalyst activity from 328 to 227 kg mol^{-1} h^{-1} (Table S3), presumably due to catalyst decomposition.[49]

To study the effects of cations on **Ni1**, we performed ethylene and MA copolymerization studies in the presence of various alkali ions using our optimized conditions at 30 °C (Table 1). The use of $MBAr^F{}_4$ is preferred over other MX salts (where X^- = BPh_4^-, $SO_3CF_3^-$, *etc.*) because the $BAr^F{}_4^-$ anion acts as a non-coordinating spectator ion.[41] Our data revealed that catalyst activity decreased from 1020 to 196 kg mol^{-1} h^{-1} whereas the MA incorporation increased from 0.71 to 1.26 mol% mostly according to the order Li^+ → Na^+ → K^+ → Cs^+ (entries 2–5). In contrast, the polymer MW did not follow an obvious trend, with **Ni1**–Li (M_n = 18.9 kg mol^{-1}) and **Ni1**–Na (M_n = 2.2 kg mol^{-1}) giving the highest and lowest, respectively. As a control, reactions in the absence of M^+ gave no products (entry 1). These results are qualitatively similar to those observed previously with **Ni1**–M in ethylene homopolymerization,[26,41] except that the catalyst activities and polymer MWs are lower in the present study due to the inhibiting effects of MA. Based on independent computational investigations of this nickel system by Ratanasak, Parasuk, and coworkers,[50] it was proposed that the energy barriers associated with the elementary steps in coordination–insertion of ethylene (*e.g.*, *cis*–*trans* nickel isomerization, olefin insertion,

Table 1 Ethylene and alkyl acrylate copolymerization using **Ni1**/cations[a]

Entry	M^+	Acrylate	Act. (kg mol^{-1} h^{-1})	Inc.[b] (mol%)	M_n[c] (kg mol^{-1})	$Đ$[c]	Acrylate/chain[d]	T_m (°C)
1	None	MA	0	—	—	—	—	—
2	Li^+	MA	1020	0.71	18.9	1.4	4.7	125
3	Na^+	MA	328	1.08	2.2	1.1	0.8	107
4	K^+	MA	340	1.12	3.1	1.4	1.2	115
5	Cs^+	MA	196	1.26	12.3	1.6	5.4	119
6	Li^+	BA	843	0.26	14.8	1.3	1.4	124
7	Na^+	BA	492	0.58	2.3	1.4	0.5	112
8	K^+	BA	467	0.76	3.7	1.8	1.0	121
9	Cs^+	BA	312	0.89	15.1	1.5	4.7	116
10	Li^+	EA	366	0.2	11.7	1.5	0.8	124

[a] Polymerization conditions: **Ni1** catalyst (2 μmol), $MBAr^F_4$ (4 μmol), $Ni(COD)_2$ (8 μmol), ethylene (400 psi), alkyl acrylate (2.5 mmol, 0.05 M), 48 mL toluene/2 mL Et_2O, 30 °C, 30 min. In the absence of cations, **Ni1** is not active for polymerization. Temperature was controlled by manual external cooling when necessary to ensure that the reaction temperature did not exceed 5 °C from the starting temperature. [b] Determined by ^1H NMR spectroscopy. See SI for the equations used. The standard deviations are typically less than 7%. [c] Determined by GPC in trichlorobenzene at 160 °C. The standard deviations are typically less than 10%. Abbreviations: MA = methyl acrylate, EA = ethyl acrylate, BA = *tert*-butyl acrylate. [d] See SI for calculations.

and olefin binding) are lowest in the presence of Li^+ and highest in the presence of Cs^+. Their density functional theory (DFT) results are consistent with our experimental observations that the catalyst activity follows the periodic trend from $Li^+ \rightarrow Na^+ \rightarrow K^+ \rightarrow Cs^+$. Our results showing that the more active **Ni1**–M catalysts yielded copolymers with lower MA mol% indicate that ethylene insertion is faster relative to MA insertion. However, further mechanistic studies of the copolymerization process are necessary to identify the rate-determining steps and evaluate whether there are cooperative interactions between MA and the metal centers in **Ni1**–M.[51,52] The **Ni1**–M catalysts were also capable of producing ethylene-ethyl acrylate (EEA) and ethylene-*tert*-butyl acrylate (EBA) copolymers from ethylene and the corresponding comonomer (Table 1, entries 6–10).

Because **Ni1**–Cs appeared to show greater thermal stability than the other **Ni1**–M catalysts, we also evaluated its activity at different temperatures (Fig. 2 and Table S4). Our results indicated that **Ni1**–Cs has maximum activity at 70 °C (512 kg mol^{-1} h^{-1}) but still gave EMA with appreciable rates at 90 °C (485 kg mol^{-1} h^{-1}). At 70 °C, the activity of **Ni1**–Cs was noticeably higher than at 30 °C, with up to 988 kg mol^{-1} h^{-1} for the copolymerization of ethylene and *tert*-butyl acrylate (Table S6).

Compared to other metal catalysts that have been reported for ethylene and alkyl acrylate copolymerization, the **Ni1**–M complexes are among the top-performers (Fig. 3; see Table S20 for more examples).[53,54] The most active nickel catalysts are all based on the phenoxyphosphine ligand platform.[22,43–45] This catalyst family includes **Ni3** with 2,6-diisopropyloxyphenyl phosphine substituents[18] and **Ni4** that is immobilized on magnesium oxide support.[55] For comparison purposes we will use **Ni1**–Li as a representative example of our cation-tunable catalysts. Based on the copolymerization data, the rankings are as follows: **Ni3** > **Ni1**–Li > **Ni4**/MgO for activity and **Ni3** > **Ni4**/MgO > **Ni1**–Li for polymer molecular weight. All three nickel catalysts gave EMA with <1.0 mol% of MA incorporation. One of the most active palladium catalysts reported for ethylene and MA copolymerization is **Pd1**,[56] which features a phosphine-phosphine oxide ligand. This palladium catalyst compares favorably with the nickel catalysts but it provided EMA with a molecular weight of only 7 kg mol^{-1}.

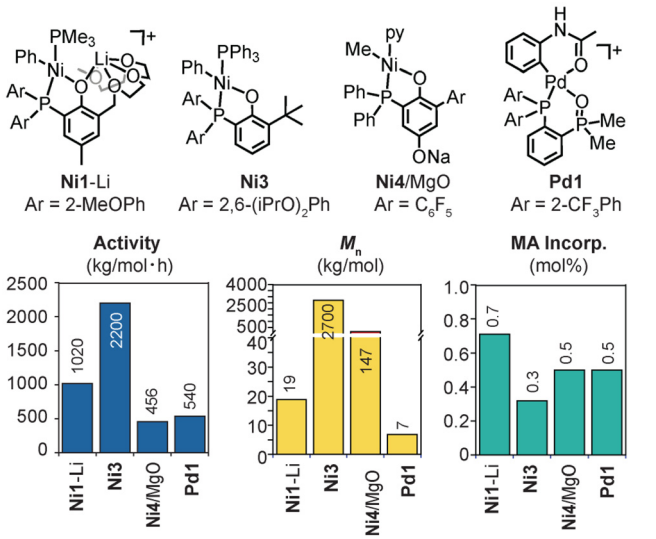

Fig. 3 Representative examples of the most active catalysts for ethylene and methyl acrylate copolymerization reported to date. See Fig. S28 and Table S20 for more examples.

Dynamic cation switching polymerization

Non-living polymerization catalysts yield a specific polymer independent of the reaction time.[57,58] However, the polymer microstructure can still be tuned by varying the experimental conditions.[34] Our method using dynamic cation switching allows regulation of non-living polymerizations without reaction engineering.[40] This strategy is distinct from those that rely on static switching[28–31] or oscillating catalysis.[59–62] Based on our success using this method for ethylene homopolymerization, we propose that dynamic cation switching can also be applied to ethylene and polar monomer copolymerization. In

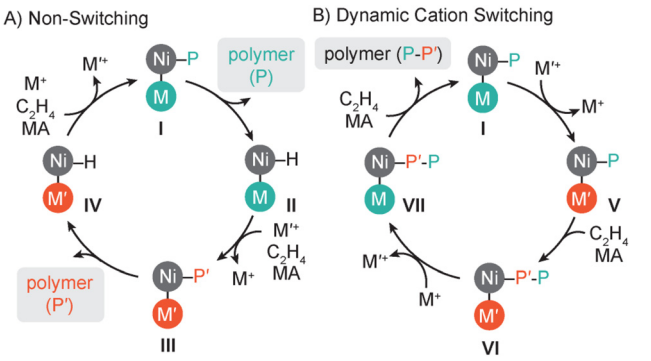

Scheme 1 Simplified catalytic cycles for non-switching (A) and dynamic cation switching (B) copolymerization of ethylene and methyl acrylate using Ni/M^+/M'^{+}. P = polymer segment controlled by Ni–M^+, P′ = polymer segment controlled by Ni–M'^{+}, MA = methyl acrylate.

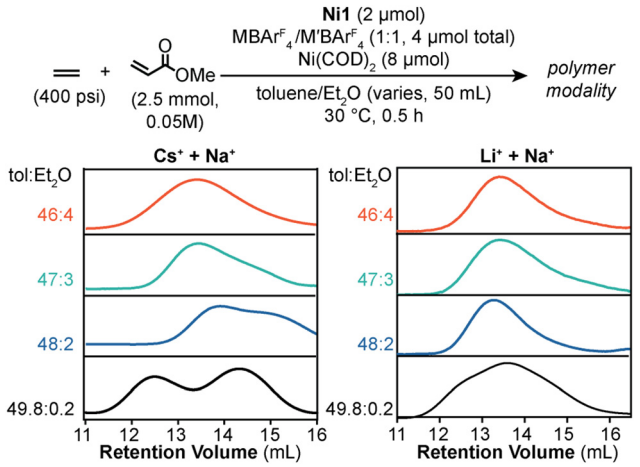

Fig. 4 Study of solvent polarity on the modality of polymers obtained from the copolymerization of ethylene and MA with **Ni1**/M^+/M'^{+}. The traces show the gel permeation chromatograms of the products obtained when different toluene/Et_2O mixtures were used. The GPC traces show signals from the refractive index detector.

non-polar solvents, we expect that combining our nickel catalyst with M^+ and M'^{+} would generate Ni(P)–M and Ni(P′)–M′ species that do not undergo cation exchange (where P and P′ = growing polymer chains, Scheme 1), which means that two different active species will copolymerize ethylene and MA independently to yield bimodal polymers. In the simplified catalytic cycle shown in Scheme 1A, the heterobimetallic Ni(P)–M (**I**) with a growing polymer chain can undergo β-hydride elimination to yield intermediate Ni(H)–M (**II**) and polymer P. Species **II** can convert to Ni(P′)–M′ (**III**) due to cation swapping of M^+ for M'^{+} and subsequent copolymerization. Chain termination from this intermediate would generate Ni(H)–M′ (**IV**) and polymer P′. Under a non-switching regime, the polymer produced will comprise P and P′ with different relative distributions depending on the M^+ : M'^{+} ratio used in the reaction.

In slightly polar solvents, we anticipate that combining our nickel catalyst with M^+ and M'^{+} would generate active nickel species that continuously cycle between Ni/M^+ and Ni/M'^{+} states during chain propagation (*i.e.*, if cation switching is faster than the termination) (Scheme 1B). For example, starting from species **I**, exchange of M^+ with M'^{+} will afford Ni(P)–M′ (**V**), which is capable of promoting further ethylene and MA insertions to **VI**. This propagating species can undergo cation exchange to **VII** as the reaction continues. Because each polymer chain is derived from a single active species that switches between two states, adjusting the M^+ : M'^{+} ratio determines the extent in which Ni/M^+ and Ni/M'^{+} controls the growth of individual polymer chains. This strategy would enable precise fine-tuning of the polymer microstructure, achieving a level of control beyond what is feasible through reaction engineering.

To determine if cation switching can occur in the presence of polar monomers, we performed ethylene and MA copolymerizations in different solvent mixtures (Fig. 4). When **Ni1** was combined with CsBAr$^F_4$/NaBAr$^F_4$ (1 : 1 ratio, 1 equiv. each relative to Ni), Ni(COD)$_2$, ethylene, and MA under standard conditions, we obtained EMA with different MWD depending on the polarity of the solvent used. The gel permeation chromatograms (GPC) showed that the EMA obtained from reactions in 49.8 : 0.2 and 48 : 2 toluene/Et_2O mixtures were bimodal whereas those obtained from reactions in 47 : 3 and 46 : 4 toluene/Et_2O mixtures were monomodal or nearly so ($Đ$ < 2.0; Fig. 4, bottom left). These results suggest that in less polar solvents, cation exchange between **Ni1**–Cs and **Ni1**–Na is slow so polymer chain growth occurs from two distinct active species. As the solvent polarity is increased, each nickel catalyst switches continuously between two different states (**Ni1**/Cs^+ and **Ni1**/Na^+) during chain propagation so only a single polymer population is produced. When this study was conducted using **Ni1** with LiBAr$^F_4$/NaBAr$^F_4$, similar results were obtained except that monomodal EMA was observed in the 48 : 2 toluene/Et_2O mixture (Fig. 4, bottom right). Because the minimum solvent polarity needed to achieve dynamic cation switching is dependent on the binding affinity of the specific cations to **Ni1**, different salt combinations will require different toluene/Et_2O mixtures. Increasing the amount of Et_2O used in the reactions decreased the catalyst activity, most likely due to the solvent serving as a competing ligand for the nickel active sites (Tables S7 and S8).

Molecular weight distribution tuning

To manipulate the copolymer MWD, we varied the Li^+ : Na^+ ratio while keeping the **Ni1**, Ni(COD)$_2$, ethylene, and MA amounts constant in a 49.8 : 0.2 mixture of toluene/Et_2O (Fig. 5 and Table S9). Analysis of the resulting EMA revealed that in all cases, bimodal polymers were obtained, in which their MWD is skewed toward the higher molecular weight end if the ratio of Li^+ : Na^+ was higher and *vice versa*. Deconvolution of the GPC traces obtained from the 3 : 1 Li^+ : Na^+ reaction showed a higher molecular weight peak A and a lower molecular weight peak B with an integrated ratio A/B of 0.86. When

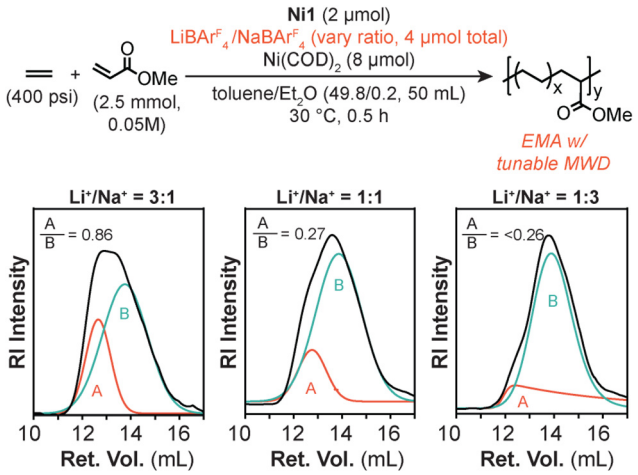

Fig. 5 Ethylene and MA copolymerization under non-switching conditions using **Ni1**, LiBAr$^F_4$, and NaBAr$^F_4$. The black trace shows the GPC data, whereas the red-orange and turquoise traces are fits from the data deconvolution. The A/B term is defined as the integration of peak A divided by the integration of peak B. Detailed polymerization results are given in Table S9.

the Li$^+$: Na$^+$ ratio was changed to 1 : 1 and 1 : 3, the A/B values dropped to 0.27 and <0.26, respectively. We were unable to fit the minor component (peak A) in the 1 : 3 Li$^+$: Na$^+$ data to a Gaussian distribution so the A/B value calculated is likely an upper limit. These results are consistent with our proposed mechanistic model (Scheme 1A) because using more Li$^+$ relative to Na$^+$ salt favors the formation of higher MW producing **Ni1**–Li over the lower MW producing **Ni1**–Na (Table 1).

Molecular weight and MA incorporation tuning

Monomodal EMA can be tailored in several ways: (1) by varying both the MW and MA incorporation; (2) by varying the MW but keeping MA incorporation constant; or (3) by varying the MA incorporation but keeping the MW constant. A desired copolymer can be synthesized as long as the target parameters fall within the ranges accessible by **Ni1**–M and **Ni1**–M′.

To achieve option 1, we used Li$^+$ and Na$^+$ salts with **Ni1** because the corresponding **Ni1**–Li and **Ni1**–Na species afford EMA with different molecular weight and MA incorporation (Table 2, entries 2–6). The copolymerizations were performed in 48 : 2 toluene : Et$_2$O to promote fast cation exchange. When greater amounts of Li$^+$ were added relative to Na$^+$, the EMA molecular weight increased gradually from ~6 to 18 kg mol^{-1} whereas the MA incorporation decreased gradually from ~1.1 to 0.7 mol% (Fig. 6A). The monomodal distributions (Fig. S11) and polymer dispersity of <2.0 strongly suggest that the products were generated by a single active species, which supports a dynamic cation switching mechanism (Scheme 1B). To achieve option 2, we paired **Ni1** with Cs$^+$ and Na$^+$ salts

Table 2 Dynamic cation switching polymerization data

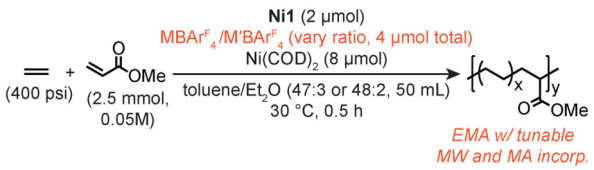

Entry[a]	M$^+$: M′$^+$ ratio		Act. (kg mol^{-1} h^{-1})	Inc.[b] (mol%)	M_n[c] (kg mol^{-1})	$Đ$[c]	MA/chain[d]	T_m[e] (°C)
1	Li$^+$: Na$^+$	2 : 0	1020	0.71	18.9	1.4	4.7	125
2	Li$^+$: Na$^+$	5 : 1	913	0.73	18.5	1.3	4.7	123
3	Li$^+$: Na$^+$	3 : 1	686	0.83	15.4	1.6	4.5	124
4	Li$^+$: Na$^+$	2 : 1	690	0.96	15.9	1.4	5.0	123
5	Li$^+$: Na$^+$	1 : 1	597	1.04	11.8	1.2	4.3	123
6	Li$^+$: Na$^+$	1 : 3	397	1.11	6.0	1.3	2.3	114
7	Li$^+$: Na$^+$	0 : 2	328	1.08	2.2	1.1	0.8	107
8	Cs$^+$: Na$^+$	2 : 0	102	1.45	17.8	1.3	8.9	117
9	Cs$^+$: Na$^+$	5 : 1	147	1.50	8.3	1.3	4.3	115
10	Cs$^+$: Na$^+$	3 : 1	154	1.43	6.6	1.7	3.2	117
11	Cs$^+$: Na$^+$	2 : 1	162	1.35	5.9	1.2	2.8	116
12	Cs$^+$: Na$^+$	1 : 1	144	1.34	4.6	1.4	2.1	113
13	Cs$^+$: Na$^+$	1 : 3	262	1.31	3.4	1.5	1.5	111
14	Cs$^+$: Na$^+$	0 : 2	266	1.15	3.1	2.3	1.2	107
15	Li$^+$: Cs$^+$	2 : 0	664	0.92	16.9	1.6	5.4	122
16	Li$^+$: Cs$^+$	5 : 1	636	1.03	18.4	1.3	6.6	123
17	Li$^+$: Cs$^+$	3 : 1	529	1.08	19.6	1.5	7.4	123
18	Li$^+$: Cs$^+$	2 : 1	522	1.14	19.1	1.3	7.6	120
19	Li$^+$: Cs$^+$	1 : 1	510	1.21	19.7	1.6	8.2	118
20	Li$^+$: Cs$^+$	1 : 3	161	1.41	20.6	1.6	10.1	118
21	Li$^+$: Cs$^+$	0 : 2	102	1.45	17.8	1.3	8.9	117

[a] The toluene : Et$_2$O ratio was 48 : 2 for Li$^+$/Na$^+$ and 47 : 3 for Cs$^+$/Na$^+$ and Li$^+$/Cs$^+$. [b] Determined by ^{1}H NMR spectroscopy. The standard deviations are typically less than 7%. [c] Determined by GPC in trichlorobenzene at 160 °C. The standard deviations are typically less than 10%. [d] See SI for equations used. [e] Measured using DSC.

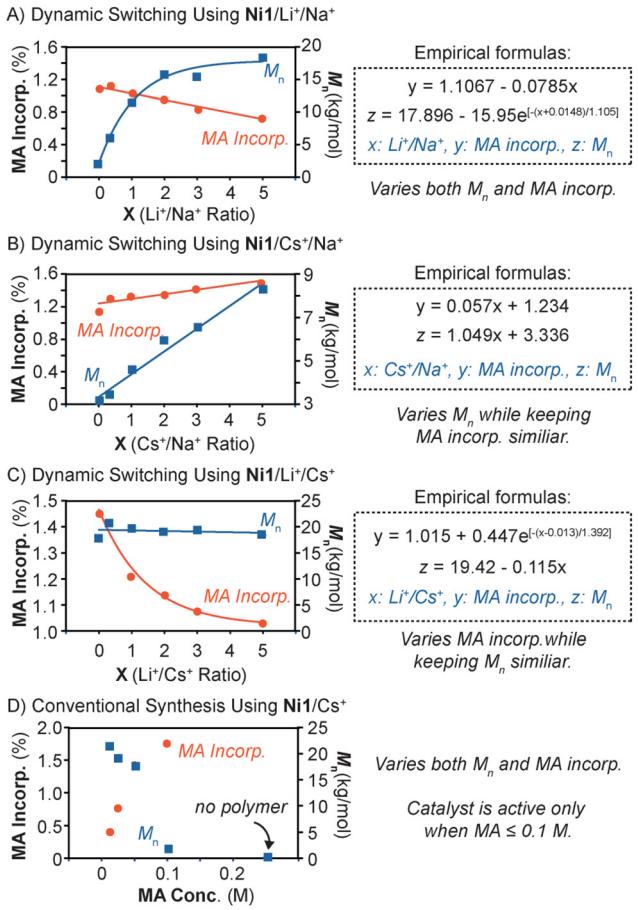

Fig. 6 Plots showing the use of Li^+/Na^+ (A), Cs^+/Na^+ (B), or Li^+/Cs^+ (C) with **Ni1** under dynamic cation switching conditions to obtain EMA with varying molecular weight and MA incorporation. For comparison, EMA synthesis was attempted by varying the MA concentration using **Ni1**–Cs (D). The empirical formulas for each polymerization set were derived from mathematical fitting. The polymerization data are provided in Tables 2 and S10–S12.

(toluene/Et_2O = 47 : 3) because the **Ni1**–Cs and **Ni1**–Na species formed will produce EMA with different MW but similar MA incorporation (Table 2, entries 9–13). Our data showed that increasing the $Cs^+ : Na^+$ ratio increased the EMA molecular weight from ~3 to 8 kg mol^{-1} while keeping the MA incorporation within a narrow range (Δincorp. = 0.2 mol% going from 1 : 3 to 5 : 1 $Cs^+ : Na^+$) (Fig. 6B). Finally, to achieve option 3, a combination of Li^+ and Cs^+ cations were used with **Ni1** (toluene/Et_2O = 47 : 3) because the resulting **Ni1**–Li and **Ni1**–Cs generated will yield EMA with similar MW but different MA incorporation. As shown in Fig. 6C, increasing Li^+ relative to Cs^+ generated copolymers featuring an average M_n of ~19 kg mol^{-1} but decreasing MA incorporation from 1.4 to 1.0 mol% (Table 2, entries 16–20).

The data above were fit to mathematical functions, providing empirically derived formulas for calculating the amount of M^+ and M'^+ salts needed to obtain copolymers with a specific set of characteristics (Fig. 6A–C).[40] Equations correlating "*z*" (M_n) with "*x*" (M^+/M'^+ molar fraction) and "*y*" (MA incorporation) with "*x*" were determined for each **Ni1**/M^+/M'^+ combination. Three-dimensional exponential and/or polynomial equations can be used to relate all 3 variables (*x*, *y*, and *z*) and are given in the SI (Fig. S16, S19, and S22). Although theoretical modeling of the experimental data may be possible, it would be difficult given that the rates of various elementary steps and cation association/dissociation processes are needed to fully describe the polymerization process. These empirical relationships are useful because they allow prediction of the polymer products attainable using any combination of **Ni1**/M^+/M'^+ that has been tested (Table S13).

To compare the effectiveness of our strategy *vs.* that of a typical approach to customize EMA, we carried out ethylene and MA copolymerization using **Ni1**–Cs under standard conditions but with varying concentrations of the polar monomer (Fig. 6D and Table S14). We observed that increasing the MA concentration from 0.01 to 0.10 M afforded EMA with decreasing molecular weight (21 to 6 kg mol^{-1}) but increasing MA incorporation (0.42 to 1.77 mol%). The inverse relationship between polymer MW and MA incorporation is expected because the presence of acrylates can induces faster chain termination.[44] At higher MA concentration, the **Ni1**–Cs activity dropped significantly, from 532 to 46 kg mol^{-1} h^{-1}. When 0.25 M methyl acrylate was used, the catalyst was completely inactive. These results are consistent with previous studies showing that polar monomers can inhibit polymerization through engaging in σ interactions with the metal catalyst.[63] Because our strategy does not require changing the MA concentration to adjust the polymer composition, moderate to high activities (>100 kg mol^{-1} h^{-1}) were obtained in our copolymerizations (Table 2).

To determine the microstructures of the copolymers, we relied on characterization using ^1H and ^{13}C NMR spectroscopy. We observed that in most cases, the MA units in EMA are located primarily in-chain,[43,64,65] as revealed by the ^1H NMR signal at 3.71 ppm and the ^{13}C NMR signal at 176 ppm corresponding to the methyl and carbonyl groups of MA, respectively (Fig. S39–S49). Similarly, the ethylene/*tert*-butyl acrylate copolymers were found to also contain in-chain BA groups (Fig. S56 and S57). The exception to this trend is copolymers synthesized using more polar solvent mixtures (*e.g.*, 45 : 5 toluene : Et_2O, Fig. S65–S68), which featured both in-chain and chain-end polar moieties. Given that under our standard polymerization conditions we obtained copolymers with mostly in-chain polar groups, insertion of alkyl acrylate into the Ni-polymeryl species does not appear to induce chain termination.[44]

Although the "tunable range" in these experiments is somewhat narrow (*e.g.*, M_n between ~3 to 8 kg mol^{-1} using Cs^+/Na^+ and MA incorporation between 1.0 to 1.4 mol% using Li^+/Cs^+), this restriction is due to limitations of the **Ni1** catalyst rather than the tuning method. We expect that **Ni2** (Scheme S1),[40] which can give polyethylene with M_n of >1000 kg mol^{-1} in the presence of Cs^+, will likely afford access to EMA with a wider range of molecular weights.

Polymer properties

Because we were able to synthesize EMA with controlled MW and MA incorporation, it allowed us to systematically study their structure–function relationships. To measure the melting (T_m) and 5% mass loss (T_5) temperatures, differential scanning calorimetry (DSC) and thermal gravimetric analysis (TGA) were used, respectively. Our data revealed that the polymers' thermal properties were more dependent on its chain length than polar group density when the MA incorporation is low. For example, lowering the EMA molecular weight from 8 to 3 kg mol^{-1} while keeping MA density constant led to a maximum reduction in T_m by 6 °C and T_5 by 48 °C (Table S11). In contrast, increasing the MA incorporation from 1.0 to 1.4 mol% while maintaining a similar MW, resulted in only small changes to the EMA's thermal parameters (max ΔT_m = ~5 °C and ΔT_5 = ~9 °C) (Table S12). It should be noted that while most copolymers produced DSC and TGA traces with sharp features, samples obtained from reactions using **Ni1**/NaBAr$^F_4$ (*e.g.*, Fig. S88B and S90B) showed broad curves. Given the narrow polymer dispersity of these samples ($Đ$ < 2.0), it is possible that the irregular features may stem from having multiple crystalline domains within the polymer structure[66,67] or non-uniform distribution of the MA units.

Next, we investigated the physical properties of the copolymers as a function of MA. All measurements were performed on polymers with an average molecular weight of ~20 kg mol^{-1} and average MA incorporation of 0 (**PE-1**), 0.8 (**EMA-1**), 1.1 (**EMA-2**), and 1.4 mol% (**EMA-3**) (Table 3). The polymer specimens were molded into a T-bone shape and then subjected to tensile testing. The stress *vs.* strain curves (Fig. S24 and S25) showed that all of the materials evaluated have similar mechanical properties, with elongation at break ranging from 8–10% and tensile strength between 19–23 MPa (Table 3). These values are typical for high-density polyethylene, which can range from 3–1900% and 3–60 MPa for elongation-at-break and tensile strength, respectively.[68] Our results suggest that the presence of small amounts of MA in the polymer chain has negligible impact on its mechanical properties.

To determine the wettability of the polymer samples, their water contact angles were measured using a static drop method at 25 °C (Fig. S26).[69,70] We found that **PE-1** had an average contact angle of 107.8°, which is within the range expected for polyethylene.[71,72] When the methyl acrylate content increased to 7 (**EMA-1**), 8 (**EMA-2**), and 10 (**EMA-3**) units per chain, the water contact angle decreased to 99.6, 97.8, and 94.0°, respectively (Table 3), indicating that the EMA-coated surface became increasingly more polar.[4,73–75]

Polymer degradability

It has been shown that functional polyolefins can be degraded under oxidative conditions[65] but quantitative correlations between the polar group density and polymer degradability have not yet been clearly established. Studying such relationships requires access to copolymers with the same MW that vary only in their polar group content to prevent conflating other factors that may contribute to degradability. With our newly synthesized polymers in hand, we had the opportunity to investigate how functional groups within the polyolefin chain influence its susceptibility toward oxidative degradation.[76–78] Although a variety of methods are available to cleave the inert C–C bonds in polyolefins, such as thermal cracking,[79–81] dehydrogenation/metathesis,[82] or dehydrogenation/isomerization/ethenolysis,[83,84] they typically require high temperatures (>150 °C) and/or precious metal catalysts.

Inspired by reports on the reactions of peroxides with polyethylene,[85–87] we focused on developing polymer degradation methods that can be performed under mild oxidizing conditions. We found that stirring **PE-1**, **EMA-1**, **EMA-2**, or **EMA-3** in the presence of *tert*-butylperoxy-2-ethylhexyl carbonate (TBEC) in H_2O at 75 °C for 24 h was sufficient to promote polymer degradation (Fig. 7A). The solid products were isolated by filtration, washed with water and acetone, and then dried overnight. The recovered mass was up to ~90% of the starting mass (Table S17), suggesting that the material isolated represents the bulk of the TBEC-treated products. To determine the extent of degradation, we analyzed the products by GPC and calculated the reduction in molecular weight percentage (ΔM_n) using the formula: $(MW_i - MW_f)/MW_i \times 100\%$, in which MW_i is the initial molecular weight and MW_f is the final molecular weight (Table S17). In the absence of peroxide, the ΔM_n did not exceed ~15% regardless of whether the polymer contained MA (Fig. 7A). In contrast, the addition of TBEC to the reactions led to significant changes in polymer molecular weight. For example, **PE-1** had an average ΔM_n value of 74% and **EMA-1**, **EMA-2**, and **EMA-3** had average ΔM_n values of 88, 92, and 97%, respectively. The peroxide indices (PI), defined as ΔM_n in the presence of peroxide divided by ΔM_n in the absence of peroxide, were 5.0, 7.9, 7.6, and 12.9, respectively (Table 3). These results indicated that: (1) appreciable polymer

Table 3 Polymer characterization data (averaged)[a]

Polymer	Inc. (%)	MA per chain	M_n (kg mol^{-1})	Elong. at break (%)	Tensile strength (MPa)	Contact angle (°)	PI
PE-1	0	0	19	9.2	19.7	107.8	5
EMA-1	0.8	6.6	23	10.4	23.2	99.6	7.9
EMA-2	1.1	7.8	20	10.5	21.2	97.8	7.6
EMA-3	1.4	10.5	21	8.4	20.1	94.0	16.4

[a] Values shown are the average from two independently prepared samples with similar MA incorporation and M_n. The maximum standard deviations is ±0.1 mol% for MA incorporation and ±2 kg mol^{-1} for MW. See Table S18 for more details. PI = peroxide index.

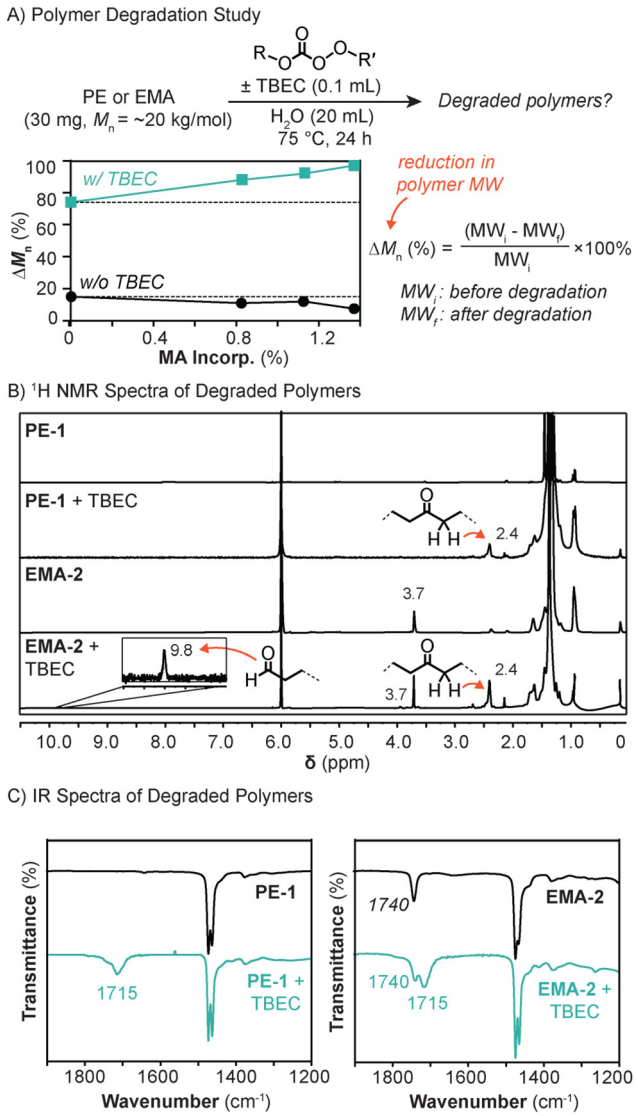

Fig. 7 Comparison of polymer MW with and without TBEC treatment after thermal degradation (A). The ^{1}H NMR (B) and IR (C) spectra of the starting and degraded polymers are provided. The ^{1}H NMR peak at 3.7 ppm is assigned to the methyl hydrogens in the methyl ester group. See Fig. S101 for the GPC traces.

degradation occurred only under oxidative conditions and (2) the polymer degradation efficiency was enhanced upon introducing more MA per chain, requiring only 1–3 units to achieve measurable effects.

To determine whether the presence of EMA can enhance the degradability of PE, we combined both polymers (1 : 1 mixture of PE and EMA containing 1.0 mol% MA; average M_n = 18.7 kg mol^{-1}) in H_2O with TBEC and stirred the sample for 24 h at 75 °C (Table S17). Our results showed that the average ΔM_n was about 82%, which is higher than that for PE (74%) but lower than that for EMA containing 1.0 mol% MA (~90%) (Fig. S101). Interestingly, this ΔM_n value is expected for EMA containing 0.5 mol% polar density. Thus, these results indicate that the degradation efficiency can be predicted based on the total MA composition in a polymer mixture, regardless of whether the polar groups are located on the same chain.

The TBEC-treated polymers were further characterized to determine their composition. ^{1}H NMR spectroscopic analysis of the degraded **PE-1** product showed a new peak at ~2.4 ppm that was assigned to α-keto hydrogens (~0.75 mol%; Fig. 7B and S83).[65] The ^{1}H NMR spectrum of degraded **EMA-2** exhibited new peaks at 2.4 and 9.8 ppm, which were attributed to α-keto (~1.0 mol%) and aldehyde (<0.1 mol%) hydrogens, respectively (Fig. 7B and S85). The MA content in degraded **EMA-2** dropped from ~1.1 to 0.5 mol%. Signals corresponding to C–H hydrogens from alcohol moieties (~3.6 ppm) were not detected in any of the samples. Attempts to observe the C=O peaks in the ^{13}C NMR spectra were unsuccessful (Fig. S100), most likely due to the low concentration of carbonyl groups in the polymer samples and their inherently weak NMR signals.

To support the NMR spectral assignments, we also measured the infrared (IR) spectra of the degraded polymers. Comparison of the vibrational data for **PE-1** before and after treatment with TBEC, revealed a new peak at 1715 cm^{-1} that corresponds to the C=O stretch of ketone groups (Fig. 7C, left). The IR spectrum of degraded **EMA-2** also exhibited a ketone peak at 1715 cm^{-1}, along with an ester peak at 1740 cm^{-1}, suggesting that some of the methyl ester groups were intact (Fig. 7C, right).[88] The presence of O–H stretches between ~2500–3500 cm^{-1} corresponding to alcohol or carboxylic acid moieties were not detected.

Based on other studies of polymer degradation, the products observed suggest that TBEC-induced chain scission likely proceeded through a radical oxidation mechanism (Scheme S4).[89,90] Such sequences are typically initiated by H-atom abstraction by a reactive oxygen species,[85] followed by propagation involving oxygenation and homolytic O–O or C–C bond scission. Given the absence of molecular weight increase and gelation in our samples, cross-linking through radical chain recombination did not appear to occur. Unlike work reported by Nozaki and coworkers on the use of dioxygen, a cerium catalyst, and visible light to degrade carboxylated polyethylene, which generated products with ketone, aldehyde, alcohol, and carboxylic acid groups,[65] our TBEC-based method afforded products with only ketone and minor amounts of aldehyde in EMA. We hypothesize that the enhanced degradability of EMA relative to that of PE is due to the weakening of the C–H and C–C bonds in close proximity to the polar group, which makes undergoing radical reactions more facile. The high mass recovery in our degradation studies suggests that overoxidation to CO_2 is suppressed. To add value to the degraded PE and EMA products, it may be possible to convert them to paraffin waxes (C_{20}–C_{30})[91] or cross-link them with reversible linkers (*e.g.*, by using α,ω-diaminoalkane to condense with the carbonyl groups in the degraded polymers) to construct chemically-recyclable materials.[92,93] Additionally, the ketone groups can be converted to esters through Baeyer–Villiger oxidation[94–96] or treated with hydroxylamine to form amides *via* Beckmann rearrangement.[96,97]

Conclusions

In summary, we have developed a method using dynamic cation switching polymerization to obtain ethylene and alkyl acrylate copolymers with exceptional control. Our studies showed that the presence of up to 0.05 M methyl acrylate did not negatively impact cation exchange between alkali ions and **Ni1**, suggesting that this catalyst system is compatible with polar monomers. We demonstrated that the **Ni1**–M complexes are active for ethylene and alkyl acrylate (MA, EA, or BA) copolymerization, with **Ni1**–Li exhibiting activity comparable to that of the best-performing catalysts reported in the literature. Using **Ni1** and a mixture of M^+ and M'^{n+} salts, we synthesized EMA with different MWD depending on the solvent polarity (*e.g.*, 49.8 : 0.2 toluene/Et_2O gave bimodal EMA whereas 47 : 3 toluene/Et_2O gave monomodal EMA) and $M^+ : M'^{n+}$ ratio. To demonstrate the utility of our method, we successfully prepared three sets of copolymers: (1) EMA with different MW and MA incorporation; (2) EMA with different MW but similar MA incorporation; and (3) EMA with different MA incorporation but similar MW. When we attempted to tune the polar group density by increasing the MA concentration, the resulting copolymers had higher MA incorporation but reduced MW. Using larger amounts of MA had detrimental effects on the catalyst activity because MA can inhibit the catalyst *via* σ-coordination. These results suggest that dynamic cation switching polymerization affords a much higher level of control over the polymerization outcome compared to other approaches that rely on reaction optimization or engineering, which can be particularly useful in situations where the reaction conditions needed are impractical to achieve (*e.g.*, in industrial reactors that are designed to operate within certain temperatures or pressures). Free radical and coordination–insertion polymerization are complementary methods, as the former enables the synthesis of copolymers with high polar group content (*e.g.*, >50 mol%) whereas the latter is better suited for generating copolymers with lower polar group content (*e.g.*, <5 mol%).

Although low-polarity polyethylene has not traditionally been regarded as a valuable material, our research indicates that they exhibit unique and useful properties worthy of further investigations. For example, studies of **PE-1**, **EMA-1**, **EMA-2**, and **EMA-3** demonstrated that the copolymers had similar thermal and mechanical properties as those in the ethylene homopolymer but exhibit greater wettability, which could enhance their adhesiveness and compatibility with other materials. Our finding that only minor quantities of MA per chain are sufficient to increase their susceptibility toward oxidative chain scission is significant, suggesting that polymers could be engineered to be both polyethylene-like and degradable on demand, offering a possible solution to the polymer pollution problem associated with PE.[98,99] Finally, this work illustrates how advances in polymer synthesis enable the preparation of previously inaccessible materials for fundamental studies and discovery of unexpected polymer properties.

Author contributions

T. G. and L. C. R. D. C.: contributed to investigation, data analysis, visualization, and writing; R. A.: contributed to data analysis; L. H. D.: contributed to conceptualization, data analysis, writing, visualization, and supervision.

Conflicts of interest

T. G., L. C. R. D. C., and L. H. D. have a provisional patent application related to this work that is pending (U.S. Pat. Appl. No. 19/238,788).

Data availability

The data supporting this article have been included as part of the supplementary information (SI). Supplementary information: experimental procedures, synthesis and characterization, polymerization results, rheological data, and degradation studies. See DOI: https://doi.org/10.1039/d5py00819k.

Acknowledgements

We are grateful to the National Science Foundation for funding this work (CHE-2154532). We thank Dr. Ugur Aslan and Prof. Megan Robertson for assistance with polymer tensile testing, Ruwanthi Amarasekara for advice on performing water contact angle measurements, and Prof. Eva Harth for access to DSC/TGA instruments in the Center for Excellence in Polymer Chemistry sponsored by The Welch Foundation (H-E-0041).

References

1 Polyolefin Market. Roots Analysis. https://www.rootsanalysis.com/polyolefin-market (accessed March 2025).
2 G. Zanchin and G. Leone, Polyolefin thermoplastic elastomers from polymerization catalysis: Advantages, pitfalls and future challenges, *Prog. Polym. Sci.*, 2021, **113**, 101342.
3 D. Feldman, Polyolefin, olefin copolymers and polyolefin polyblend nanocomposites, *J. Macromol. Sci., Part A:Pure Appl. Chem.*, 2016, **53**, 651–658.
4 J. Kruszynski, W. Nowicka, F. A. Pasha, L. Yang, A. Rozanski, M. Bouyahyi, R. Kleppinger, L. Jasinska-Walc and R. Duchateau, Tuning the Adhesive Strength of Functionalized Polyolefin-Based Hot Melt Adhesives: Unexpected Results Leading to New Opportunities, *Macromolecules*, 2025, **58**, 2894.
5 T. C. M. Chung, Functional Polyolefins for Energy Applications, *Macromolecules*, 2013, **46**, 6671–6698.
6 L. Jasinska-Walc, M. Bouyahyi and R. Duchateau, Potential of Functionalized Polyolefins in a Sustainable Polymer Economy: Synthetic Strategies and Applications, *Acc. Chem. Res.*, 2022, **55**, 1985–1996.

7 ELVALOY Copolymers. Dow. https://www.dow.com/en-us/brand/elvaloy.html (accessed March 2025).
8 Repsol Ebantix. Repsol. https://www.repsol.com/en/products-and-services/materials/product-range/eva-and-eba/index.cshtml (accessed March 2025).
9 Optema EMA Copolymers. ExxonMobil. https://www.exxonmobilchemical.com/en/products/polyethylene/ema-copolymer (accessed March 2025).
10 D. Jeremic, Polyethylene, in *Ullmann's Encyclopedia of Industrial Chemistry*, 2014, pp. 1–42.
11 E. Y.-X. Chen, Coordination Polymerization of Polar Vinyl Monomers by Single-Site Metal Catalysts, *Chem. Rev.*, 2009, **109**, 5157–5214.
12 Z. Chen and M. Brookhart, Exploring Ethylene/Polar Vinyl Monomer Copolymerizations Using Ni and Pd α-Diimine Catalysts, *Acc. Chem. Res.*, 2018, **51**, 1831–1839.
13 A. Keyes, H. E. Basbug Alhan, E. Ordonez, U. Ha, D. B. Beezer, H. Dau, Y.-S. Liu, E. Tsogtgerel, G. R. Jones and E. Harth, Olefins and Vinyl Polar Monomers: Bridging the Gap for Next Generation Materials, *Angew. Chem., Int. Ed.*, 2019, **58**, 12370–12391.
14 J. Chen, Y. Gao and T. J. Marks, Early Transition Metal Catalysis for Olefin–Polar Monomer Copolymerization, *Angew. Chem., Int. Ed.*, 2020, **59**, 14726–14735.
15 Y. Jiang, Z. Zhang, H. Jiang, Q. Wang, S. Li and D. Cui, Polar Group-Promoted Copolymerization of Ethylene with Polar Olefins, *Macromolecules*, 2023, **56**, 1547–1553.
16 Q. Wang, M. Chen, C. Zou and C. Chen, Direct Synthesis of Polar-Functionalized Polyolefin Elastomers, *Angew. Chem., Int. Ed.*, 2025, e202423814.
17 H. Zheng, Z. Qiu, D. Li, L. Pei and H. Gao, Advance on nickel- and palladium-catalyzed insertion copolymerization of ethylene and acrylate monomers, *J. Polym. Sci.*, 2023, **61**, 2987–3021.
18 Q. Yang, X. Kang, Y. Liu, H. Mu and Z. Jian, Ultrahigh Molecular Weight Ethylene–Acrylate Copolymers Synthesized with Highly Active Neutral Nickel Catalysts, *Angew. Chem., Int. Ed.*, 2025, e202421904.
19 X. Sui, S. Dai and C. Chen, Ethylene Polymerization and Copolymerization with Polar Monomers by Cationic Phosphine Phosphonic Amide Palladium Complexes, *ACS Catal.*, 2015, **5**, 5932–5937.
20 N. D. Contrella, J. R. Sampson and R. F. Jordan, Copolymerization of Ethylene and Methyl Acrylate by Cationic Palladium Catalysts That Contain Phosphine-Diethyl Phosphonate Ancillary Ligands, *Organometallics*, 2014, **33**, 3546–3555.
21 Z. Saki, I. D'Auria, A. Dall'Anese, B. Milani and C. Pellecchia, Copolymerization of Ethylene and Methyl Acrylate by Pyridylimino Ni(II) Catalysts Affording Hyperbranched Poly(ethylene-*co*-methyl acrylate)s with Tunable Structures of the Ester Groups, *Macromolecules*, 2020, **53**, 9294–9305.
22 S. Xiong, M. M. Shoshani, X. Zhang, H. A. Spinney, A. J. Nett, B. S. Henderson, T. F. Miller III and T. Agapie, Efficient Copolymerization of Acrylate and Ethylene with Neutral P,O-Chelated Nickel Catalysts: Mechanistic Investigations of Monomer Insertion and Chelate Formation, *J. Am. Chem. Soc.*, 2021, **143**, 6516–6527.
23 L. R. Sita, Ex Uno Plures ("Out of One, Many"): New Paradigms for Expanding the Range of Polyolefins through Reversible Group Transfers, *Angew. Chem., Int. Ed.*, 2009, **48**, 2464–2472.
24 Z. Cai, D. Xiao and L. H. Do, Fine-Tuning Nickel Phenoxyimine Olefin Polymerization Catalysts: Performance Boosting by Alkali Cations, *J. Am. Chem. Soc.*, 2015, **137**, 15501–15510.
25 Z. Cai and L. H. Do, Thermally Robust Heterobimetallic Palladium–Alkali Catalysts for Ethylene and Alkyl Acrylate Copolymerization, *Organometallics*, 2018, **37**, 3874–3882.
26 T. V. Tran, Y. H. Nguyen and L. H. Do, Development of Highly Productive Nickel–Sodium Phenoxyphosphine Ethylene Polymerization Catalysts and their Reaction Temperature Profiles, *Polym. Chem.*, 2019, **10**, 3718–3721.
27 J. M. Kaiser, W. C. Anderson Jr. and B. K. Long, Photochemical Regulation of a Redox-Active Olefin Polymerization Catalyst: Controlling Polyethylene Microstructure with Visible Light, *Polym. Chem.*, 2018, **9**, 1567–1570.
28 B. Yang, W. Pang and M. Chen, Redox Control in Olefin Polymerization Catalysis by Phosphine–Sulfonate Palladium and Nickel Complexes, *Eur. J. Inorg. Chem.*, 2017, 2510–2514.
29 W. C. Anderson Jr., J. L. Rhinehart, A. G. Tennyson and B. K. Long, Redox-Active Ligands: An Advanced Tool To Modulate Polyethylene Microstructure, *J. Am. Chem. Soc.*, 2016, **138**, 774–777.
30 W. C. Anderson Jr. and B. K. Long, Modulating Polyolefin Copolymer Composition via Redox-Active Olefin Polymerization Catalysts, *ACS Macro Lett.*, 2016, **5**, 1029–1033.
31 J. M. Kaiser and B. K. Long, Recent Developments in Redox-Active Olefin Polymerization Catalysts, *Coord. Chem. Rev.*, 2018, **372**, 141–152.
32 Z. Cai, Z. Shen, X. Zhou and R. F. Jordan, Enhancement of Chain Growth and Chain Transfer Rates in Ethylene Polymerization by (Phosphine-sulfonate)PdMe Catalysts by Binding of $B(C_6F_5)_3$ to the Sulfonate Group, *ACS Catal.*, 2012, **2**, 1187–1195.
33 A. M. Johnson, N. D. Contrella, J. R. Sampson, M. Zheng and R. F. Jordan, Allosteric Effects in Ethylene Polymerization Catalysis. Enhancement of Performance of Phosphine-Phosphinate and Phosphine-Phosphonate Palladium Alkyl Catalysts by Remote Binding of $B(C_6F_5)_3$, *Organometallics*, 2017, **36**, 4990–5002.
34 T. V. Tran and L. H. Do, Tunable Modalities in Polyolefin Synthesis via Coordination Insertion Catalysis, *Eur. Polym. J.*, 2021, **142**, 110100.
35 L. Johnson, L. Wang, S. McLain, A. Bennett, K. Dobbs, E. Hauptman, A. Ionkin, S. Ittel, K. Kunitsky, W. Marshall, E. McCord, C. Radzewich, A. Rinehart, K. J. Sweetman, Y. Wang, Z. Yin and M. Brookhart, Copolymerization of

Ethylene and Acrylates by Nickel Catalysts, in *Beyond Metallocenes*, American Chemical Society, 2003, vol. 857, pp. 131–142.

36 S. Xiong, H. A. Spinney, B. C. Bailey, B. S. Henderson, A. A. Tekpor, M. R. Espinosa, P. Saha and T. Agapie, Switchable Synthesis of Ethylene/Acrylate Copolymers by a Dinickel Catalyst: Evidence for Chain Growth on Both Nickel Centers and Concepts of Cation Exchange Polymerization, *ACS Catal.*, 2024, **14**, 5260–5268.

37 S. Xiong, M. M. Shoshani, A. J. Nett, H. A. Spinney, B. S. Henderson and T. Agapie, Nickel-Based Heterometallic Catalysts for Ethylene-Acrylate Copolymerization: Interrogating Effects of Secondary Metal Additives, *Organometallics*, 2023, **42**, 2849–2855.

38 H.-C. Chiu, A. Koley, P. L. Dunn, R. J. Hue and I. A. Tonks, Ethylene Polymerization Catalyzed by Bridging Ni/Zn Heterobimetallics, *Dalton Trans.*, 2017, **46**, 5513–5517.

39 S. Akita and K. Nozaki, Copolymerization of Ethylene and Methyl Acrylate by Palladium Catalysts Bearing IzQO Ligands Containing Methoxyethyl Ether Moieties and Salt Effects for Polymerization, *Polym. J.*, 2021, **53**, 1057–1060.

40 T. V. Tran, E. Lee, Y. H. Nguyen, H. D. Nguyen and L. H. Do, Customizing Polymers by Controlling Cation Switching Dynamics in Non-Living Polymerization, *J. Am. Chem. Soc.*, 2022, **144**, 17129–17139.

41 T. V. Tran, L. J. Karas, J. I. Wu and L. H. Do, Elucidating Secondary Metal Cation Effects on Nickel Olefin Polymerization Catalysts, *ACS Catal.*, 2020, **10**, 10760–10772.

42 F. B. Ogilvie, J. M. Jenkins and J. G. Verkade, ^{31}P-^{31}P Spin-Spin Coupling in Complexes Containing Two Phosphorus Ligands, *J. Am. Chem. Soc.*, 1970, **92**, 1916–1923.

43 B. S. Xin, N. Sato, A. Tanna, Y. Oishi, Y. Konishi and F. Shimizu, Nickel Catalyzed Copolymerization of Ethylene and Alkyl Acrylates, *J. Am. Chem. Soc.*, 2017, **139**, 3611–3614.

44 S. Xiong, A. Hong, P. Ghana, B. C. Bailey, H. A. Spinney, H. Bailey, B. S. Henderson, S. Marshall and T. Agapie, Acrylate-Induced β-H Elimination in Coordination Insertion Copolymerizaton Catalyzed by Nickel, *J. Am. Chem. Soc.*, 2023, **145**, 26463–26471.

45 Y. Zhang, H. Mu, L. Pan, X. Wang and Y. Li, Robust Bulky [P,O] Neutral Nickel Catalysts for Copolymerization of Ethylene with Polar Vinyl Monomers, *ACS Catal.*, 2018, **8**, 5963–5976.

46 Y. Zhang, H. Mu, X. Wang, L. Pan and Y. Li, Elaborate Tuning in Ligand Makes a Big Difference in Catalytic Performance: Bulky Nickel Catalysts for (Co)polymerization of Ethylene with Promising Vinyl Polar Monomers, *ChemCatChem*, 2019, **11**, 2329–2340.

47 B. Tahmouresilerd, D. Xiao and L. H. Do, Rigidifying Cation-Tunable Nickel Catalysts Increases Activity and Polar Monomer Incorporation in Ethylene and Methyl Acrylate Copolymerization, *Inorg. Chem.*, 2021, **60**, 19035–19043.

48 H. Zheng, Z. Qiu, H. Gao, D. Li, Z. Cheng, G. Tu and H. Gao, Noncovalent Ni–Phenyl Interactions Promoted α-Diimine Nickel-Catalyzed Copolymerization of Ethylene and Methyl Acrylate, *Macromolecules*, 2024, **57**, 5279–5288.

49 A. Berkefeld and S. Mecking, Deactivation Pathways of Neutral Ni(II) Polymerization Catalysts, *J. Am. Chem. Soc.*, 2009, **131**, 1565–1574.

50 P. Apilardmongkol, M. Ratanasak, J.-Y. Hasegawa and V. Parasuk, Exploring the Reaction Mechanism of Heterobimetallic Nickel-Alkali Catalysts for Ethylene Polymerization: Secondary-Metal-Ligand Cooperative Catalysis, *ChemCatChem*, 2022, **14**, e202200028.

51 Z. Cai, D. Xiao and L. H. Do, Cooperative Heterobimetallic Catalysts in Coordination Insertion Polymerization, *Comments Inorg. Chem.*, 2019, **39**, 27–50.

52 J. P. McInnis, M. Delferro and T. J. Marks, Multinuclear Group 4 Catalysis: Olefin Polymerization Pathways Modified by Strong Metal–Metal Cooperative Effects, *Acc. Chem. Res.*, 2014, **47**, 2545–2557.

53 H. Mu, G. Zhou, X. Hu and Z. Jian, Recent advances in nickel mediated copolymerization of olefin with polar monomers, *Coord. Chem. Rev.*, 2021, **435**, 213802.

54 H. Mu, L. Pan, D. Song and Y. Li, Neutral Nickel Catalysts for Olefin Homo- and Copolymerization: Relationships between Catalyst Structures and Catalytic Properties, *Chem. Rev.*, 2015, **115**, 12091–12137.

55 C. Zou, G. Si and C. Chen, A general strategy for heterogenizing olefin polymerization catalysts and the synthesis of polyolefins and composites, *Nat. Commun.*, 2022, **13**, 1954.

56 Y. Mitsushige, B. P. Carrow, S. Ito and K. Nozaki, Ligand-controlled insertion regioselectivity accelerates copolymerisation of ethylene with methyl acrylate by cationic bisphosphine monoxide–palladium catalysts, *Chem. Sci.*, 2016, **7**, 737–744.

57 K. Matyjaszewski, Introduction to living polymerization. Living and/or controlled polymerization, *J. Phys. Org. Chem.*, 1995, **8**, 197–207.

58 O. W. Webster, Living Polymerization Methods, *Science*, 1991, **251**, 887–893.

59 J. C. W. Chien, G. H. Llinas, M. D. Rausch, G.-Y. Lin, H. H. Winter, J. L. Atwood and S. G. Bott, Two-State Propagation Mechanism for Propylene Polymerization Catalyzed by *rac*-[*anti*-Ethylidene(1-η^5-tetramethylcyclopentadienyl)(1-η^5-indenyl)] dimethyltitanium, *J. Am. Chem. Soc.*, 1991, **113**, 8569–8570.

60 G. H. Llinas, S. H. Dong, D. T. Mallin, M. D. Rausch, Y.-G. Lin, H. H. Winter and J. C. W. Chien, Crystalline-Amorphous Block Polypropylene and Nonsymmetric *ansa*-Metallocene Catalyzed Polymerization, *Macromolecules*, 1992, **25**, 1242–1253.

61 G. W. Coates and R. M. Waymouth, Oscillating Stereocontrol: A Strategy for the Synthesis of Thermoplastic Elastomeric Polypropylene, *Science*, 1995, **267**, 217–219.

62 V. Busico, R. Cipullo, W. P. Kretschmer, G. Talarico, M. Vacatello and V. Van Axel Castelli, "Oscillating" Metallocene Catalysts: How Do They Oscillate?, *Angew. Chem., Int. Ed.*, 2002, **41**, 505–508.

63 B. P. Carrow and K. Nozaki, Transition-Metal-Catalyzed Functional Polyolefin Synthesis: Effecting Control Through

Chelating Ancillary Ligand Design and Mechanistic Insights, *Macromolecules*, 2014, **47**, 2541–2555.
64 E. Drent, R. van Dijk, R. van Ginkel, B. van Oort and R. I. Pugh, Palladium catalysed copolymerisation of ethene with alkylacrylates: polar comonomer built into the linear polymer chain, *Chem. Commun.*, 2002, 744–745.
65 B. Lu, K. Takahashi, J. Zhou, S. Nakagawa, Y. Yamamoto, T. Katashima, N. Yoshie and K. Nozaki, Mild Catalytic Degradation of Crystalline Polyethylene Units in a Solid State Assisted by Carboxylic Acid Groups, *J. Am. Chem. Soc.*, 2024, **146**, 19599–19608.
66 T. M. Liu and I. R. Harrison, A DSC method of measuring short-chain branching distribution in linear low density polyethylene, *Thermochim. Acta*, 1994, **233**, 167–171.
67 W. Qiu, J. Sworen, M. Pyda, E. Nowak-Pyda, A. Habenschuss, K. B. Wagener and B. Wunderlich, Effect of the Precise Branching of Polyethylene at Each 21st CH_2 Group on Its Phase Transitions, Crystal Structure, and Morphology, *Macromolecules*, 2006, **39**, 204–217.
68 Overview of materials for High Density Polyethylene (HDPE). MatWeb. https://www.matweb.com/search/datasheet_print.aspx?matguid=482765fad3b443169ec28fb6f9606660 (accessed March 2025).
69 T. Huhtamäki, X. Tian, J. T. Korhonen and R. H. A. Ras, Surface-wetting characterization using contact-angle measurements, *Nat. Protoc.*, 2018, **13**, 1521–1538.
70 R. S. Hebbar, A. M. Isloor and A. F. Ismail, Chapter 12 - Contact Angle Measurements, in *Membrane Characterization*, ed. N. Hilal, A. F. Ismail, T. Matsuura and D. Oatley-Radcliffe, Elsevier, 2017, pp. 219–255.
71 W. Wang, N. Nie, M. Xu and C. Zou, Lewis acid modulation in phosphorus phenol nickel catalyzed ethylene polymerization and copolymerization, *Polym. Chem.*, 2023, **14**, 4933–4939.
72 Y. Na and C. Chen, Catechol-Functionalized Polyolefins, *Angew. Chem., Int. Ed.*, 2020, **59**, 7953–7959.
73 D. M. Brewis and D. Briggs, Adhesion to polyethylene and polypropylene, *Polymer*, 1981, **22**, 7–16.
74 Y. Shiraki, M. Saito, N. L. Yamada, K. Ito and H. Yokoyama, Adhesion to Untreated Polyethylene and Polypropylene by Needle-like Polyolefin Crystals, *Macromolecules*, 2023, **56**, 2429–2436.
75 S. N. Rusanova, S. Y. Sof'ina, A. R. Khuzakhanov, M. V. Kolpakova and O. V. Stoyanov, Adhesion Properties of Polyethylene and Ethylene-Vinyl Acetate Copolymer Blend with Acrylate Copolymers of Ethylene, *Polym. Sci., Ser. D*, 2022, **15**, 494–498.
76 D. G. H. Ballard and J. V. Dawkins, Catalytic oxidative degradation of polyethylene crystals, *Eur. Polym. J.*, 1974, **10**, 829–835.
77 H. Qin, C. Zhao, S. Zhang, G. Chen and M. Yang, Photo-oxidative degradation of polyethylene/montmorillonite nanocomposite, *Polym. Degrad. Stab.*, 2003, **81**, 497–500.
78 M. Hakkarainen and A.-C. Albertsson, Environmental Degradation of Polyethylene, in *Long Term Properties of Polyolefins*, ed. A.-C. Albertsson, Springer Berlin Heidelberg, Berlin, Heidelberg, 2004, pp. 177–199.
79 I. Ahmad, M. I. Khan, H. Khan, M. Ishaq, R. Tariq, K. Gul and W. Ahmad, Pyrolysis Study of Polypropylene and Polyethylene Into Premium Oil Products, *Int. J. Green Energy*, 2015, **12**, 663–671.
80 R. Miandad, M. A. Barakat, A. S. Aburiazaiza, M. Rehan, I. M. I. Ismail and A. S. Nizami, Effect of plastic waste types on pyrolysis liquid oil, *Int. Biodeterior. Biodegrad.*, 2017, **119**, 239–252.
81 S. C. Kosloski-Oh, Z. A. Wood, Y. Manjarrez, J. P. de los Rios and M. E. Fieser, Catalytic methods for chemical recycling or upcycling of commercial polymers, *Mater. Horiz.*, 2021, **8**, 1084–1129.
82 A. Arroyave, S. Cui, J. C. Lopez, A. L. Kocen, A. M. LaPointe, M. Delferro and G. W. Coates, Catalytic Chemical Recycling of Post-Consumer Polyethylene, *J. Am. Chem. Soc.*, 2022, **144**, 23280–23285.
83 R. J. Conk, S. Hanna, J. X. Shi, J. Yang, N. R. Ciccia, L. Qi, B. J. Bloomer, S. Heuvel, T. Wills, J. Su, A. T. Bell and J. F. Hartwig, Catalytic deconstruction of waste polyethylene with ethylene to form propylene, *Science*, 2022, **377**, 1561–1566.
84 N. M. Wang, G. Strong, V. DaSilva, L. Gao, R. Huacuja, I. A. Konstantinov, M. S. Rosen, A. J. Nett, S. Ewart, R. Geyer, S. L. Scott and D. Guironnet, Chemical Recycling of Polyethylene by Tandem Catalytic Conversion to Propylene, *J. Am. Chem. Soc.*, 2022, **144**, 18526–18531.
85 G. E. Garrett, E. Mueller, D. A. Pratt and J. S. Parent, Reactivity of Polyolefins toward Cumyloxy Radical: Yields and Regioselectivity of Hydrogen Atom Transfer, *Macromolecules*, 2014, **47**, 544–551.
86 U. Yolsal, T. J. Neal, J. A. Richards, J. R. Royer and J. A. Garden, A versatile modification strategy to enhance polyethylene properties through solution-state peroxide modifications, *Polym. Chem.*, 2024, **15**, 1399–1412.
87 T. Bremner and A. Rudin, Peroxide modification of linear low-density polyethylene: A comparison of dialkyl peroxides, *J. Appl. Polym. Sci.*, 1993, **49**, 785–798.
88 N. Huang and J. Wang, A TGA-FTIR study on the effect of $CaCO_3$ on the thermal degradation of EBA copolymer, *J. Anal. Appl. Pyrolysis*, 2009, **84**, 124–130.
89 G. Gryn'ova, J. L. Hodgson and M. L. Coote, Revising the mechanism of polymer autooxidation, *Org. Biomol. Chem.*, 2011, **9**, 480–490.
90 P. Bracco, L. Costa, M. P. Luda and N. Billingham, A review of experimental studies of the role of free-radicals in polyethylene oxidation, *Polym. Degrad. Stab.*, 2018, **155**, 67–83.
91 J. G. Speight, Chapter 3 - Hydrocarbons from Petroleum, in *Handbook of Industrial Hydrocarbon Processes*, ed. J. G. Speight, Gulf Professional Publishing, Boston, 2011, pp. 85–126.
92 D. J. Fortman, J. P. Brutman, G. X. De Hoe, R. L. Snyder, W. R. Dichtel and M. A. Hillmyer, Approaches to Sustainable and Continually Recyclable Cross-Linked Polymers, *ACS Sustainable Chem. Eng.*, 2018, **6**, 11145–11159.

93 M. Hong and E. Y. X. Chen, Chemically recyclable polymers: a circular economy approach to sustainability, *Green Chem.*, 2017, **19**, 3692–3706.
94 P. Ma, C. M. Plummer, W. Luo, J. Pang, Y. Chen and L. Li, Exhaustive Baeyer–Villiger oxidation: a tailor-made post-polymerization modification to access challenging poly (vinyl acetate) copolymers, *Chem. Sci.*, 2022, **13**, 11746–11754.
95 M. Baur, N. K. Mast, J. P. Brahm, R. Habé, T. O. Morgen and S. Mecking, High-Density Polyethylene with In-Chain Photolyzable and Hydrolyzable Groups Enabling Recycling and Degradation, *Angew. Chem., Int. Ed.*, 2023, **62**, e202310990.
96 R. Lemmens, J. Vercammen, L. Van Belleghem and D. De Vos, Upcycling polyethylene into closed-loop recyclable polymers through titanosilicate catalyzed C-H oxidation and in-chain heteroatom insertion, *Nat. Commun.*, 2024, **15**, 9188.
97 J. X. Shi, D. D. Kim, N. R. Ciccia, P. Lahaie-Boivin and J. F. Hartwig, Backbone editing and deconstruction of polyethylene by Beckmann rearrangement and hydrogenolysis, *Chem. Sci.*, 2025, **16**, 11304–11310.
98 J. M. Millican and S. Agarwal, Plastic Pollution: A Material Problem?, *Macromolecules*, 2021, **54**, 4455–4469.
99 C. J. Rhodes, Plastic Pollution and Potential Solutions, *Sci. Prog.*, 2018, **101**, 207–260.